energy&fuels

Article

pubs.acs.org/EF

Carbon Dioxide Separation from Nitrogen/Hydrogen Mixtures over Activated Carbon Beads: Adsorption Isotherms and Breakthrough Studies

Simon J. Caldwell,[†] Bushra Al-Duri,[†] Nannan Sun,[‡] Cheng-gong Sun,[‡] Colin E. Snape,[‡] Kaixi Li,[§] and Joseph Wood*[,†]

[†]School of Chemical Engineering, University of Birmingham, Edgbaston, Birmingham B15 2TT, United Kingdom

[‡]School of Chemical and Environmental Engineering, University of Nottingham, University Park, Nottingham NG7 2RD, United Kingdom

[§]Institute of Coal Chemistry, Chinese Academy of Sciences, Post Office Box 165, Tiayuan, Shanxi 030001, People's Republic of China

Supporting Information

ABSTRACT: The high-pressure separation of carbon dioxide/nitrogen and carbon dioxide/hydrogen mixtures was investigated over two phenolic-resin-derived activated carbon bead samples: an unmodified activated carbon made from a phenolic resin precursor and a modified material manufactured by treating the former activated carbon with first nitric acid and then ammonia. Equilibrium tests on the material were performed with a high-pressure volumetric analysis with carbon dioxide and nitrogen. The dynamic response of the separation was tested using a fixed-bed rig to produce carbon dioxide breakthrough curves with several carbon dioxide feed fractions (0.1, 0.2, 0.3, 0.4, and 0.5) in nitrogen. This study represents one of the few studies that equilibrium capacities have been related to the breakthrough capacities achieved in packed-bed operation for high-pressure carbon dioxide capture applications and the first to apply the ideal adsorbed solution theory (IAST) model. The equilibrium tests showed that the Langmuir−Freundlich isotherm and the dual-site Langmuir isotherm gave a closer fit to all of the data than the Langmuir isotherm alone in the pure component adsorption studies. The capacity of the material based on the dynamic separation was found with mole fractions of 0.5 carbon dioxide in nitrogen leading to 6.09 mol kg^{-1} carbon dioxide being captured over the unmodified activated carbon and 7.48 mol kg^{-1} being captured over the modified activated carbon at 25 bar and 25 °C. By comparison, the saturation capacity of the modified activated carbon in the Langmuir−Freundlich fit to the high-pressure volumetric adsorption data for 0.5 mole fraction carbon dioxide at the same temperature was 8.06 mol kg^{-1} for the unmodified material and 7.68 mol kg^{-1} for the modified material based on the pure component isotherm parameters. The breakthrough capacities were also found for feed fractions of carbon dioxide in the range of 0.1−0.5. A comparison between the dynamic capacities and those predicted by the isotherm show that pure component data are not necessarily representative of a dynamic multi-component system. Therefore, multi-component isotherm models were fitted to the data and compared to predictions using the IAST. A multi-component dual-site Langmuir equation was found to give the best fit to the binary component data. Breakthrough curves were also reported for carbon dioxide in hydrogen over the modified activated carbon, with the carbon beads showing considerable potential for application for carbon capture in pre-combustion separation units of power plants, because of their physically strength, meaning no further agglomeration of powdered samples is required for their use in packed beds.

1. INTRODUCTION

There is an increasing consensus that rising carbon dioxide emissions are leading to anthropogenic global warming. Global emissions are estimated to have been 33.3 gigatons of CO_2 for 2011, with 29% of these emission from China, 16% from the United States, and 12% from the European Union.[1] In the U.K., the power sector was responsible for 28% of all emissions,[2] and the European Union roadmap for reducing carbon emissions suggests that the biggest sector cut by both 2030 and 2050 needs to occur within the power sector.[3] As a point source of CO_2, the power industry provides the opportunity to use carbon dioxide capture and storage (CCS). It is estimated that the most economical combination of CO_2 reduction technologies will require CCS to account for 14% of the CO_2 reductions.[4]

Coal is one of the most abundant fossil fuels on earth, with sufficient reserves for over 200 years of generation at current consumption rates.[5] However, it is also responsible for the largest proportion of CO_2 emissions.[4] Pre-combustion carbon dioxide capture is becoming of increasing interest in the coal industry. Although integrated gasification combined cycle (IGCC) power stations are not as efficient as supercritical power plants, they offer greater flexibility for startup and shutdown. Furthermore, the pre-combustion carbon dioxide capture is readily achievable because the syngas produced has high concentrations of CO_2 and is at high pressures. These conditions are much more favorable for CO_2 removal than

Received: January 22, 2015
Revised: May 19, 2015
Published: May 26, 2015

DOI: 10.1021/acs.energyfuels.5b00164
Energy Fuels 2015, 29, 3796−3807

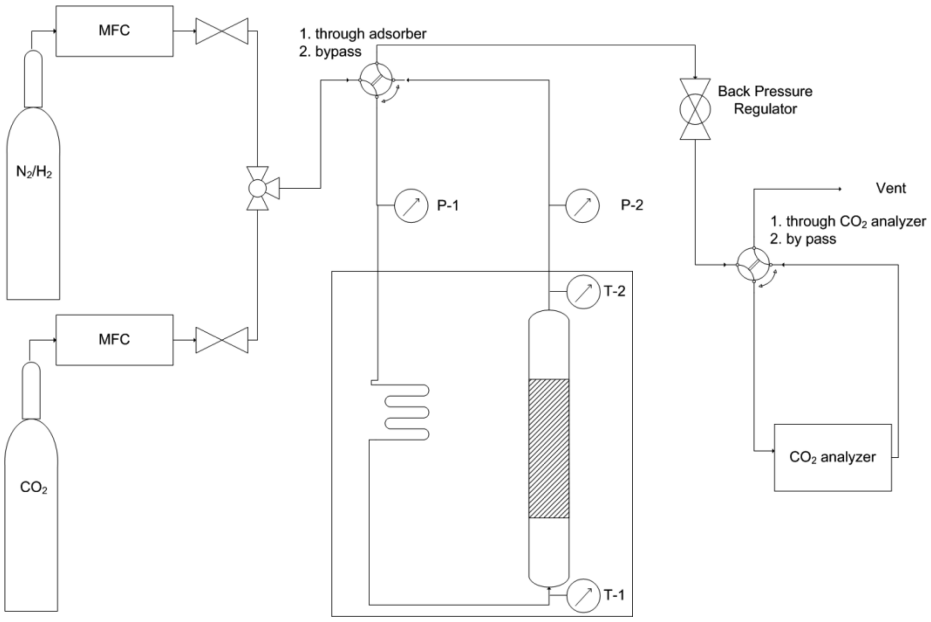

Figure 1. Experimental setup of the fixed-bed adsorption rig.

would be expected in post-combustion capture situations.[6] Current state-of-the-art acid gas removal in IGCC processes is performed using physical solvents, typically Selexol or Rectisol. Despite being more efficient than chemical solvents, there is still a significant energy penalty; therefore, higher performance and less costly acid gas removal processes need to be developed and demonstrated.[7]

Solid adsorbent processes are an alternative to liquid absorbent processes, which have been proposed to be less expensive and more efficient.[8] However, the bulk of the research has concentrated on post-combustion systems for retrofit applications. Pre-combustion capture removes carbon dioxide from high-pressure streams with a high carbon dioxide concentration, with Cormos et al.[9] giving shifted syngas conditions of 34.3 bar and a carbon dioxide volumetric fraction of 39.9%. These conditions allow for physical sorbents to be used, which do not require the same strong basic functionality required for chemical sorption.[10] Activated carbons have a large surface area and, thus, have high capacities for carbon dioxide, are low cost, and easy to regenerate.[11] They are preferred to zeolites because they have a lower adsorption strength, allowing easier desorption, and are also moisture-tolerant.[12] The work by Sun et al.[13] showed that phenolic-resin-derived activated carbon beads had capacities for CO_2 of 25−40 wt % at 40 bar as well as fast adsorption kinetics, showing their suitability for pre-combustion capture. The advantage of these adsorbents is their high physical strength, and no further agglomeration is required for their use in packed beds in pressure swing adsorption (PSA) systems. Indeed, the large-scale application of PSA for the separation of H_2 and CO_2 has been demonstrated at the Puertellano IGCC power plant in Spain owned by ELCOGAS.[14] The hydrogen purification unit obtains hydrogen with 99.99% purity from raw hydrogen coming from the separation unit. The PSA steps consist of an adsorption multi-bed system containing activated carbon, alumina, and a molecular sieve.

To date, only a handful of studies have investigated the application of activated carbons to pre-combustion systems.[10,13,15−18] Even less have considered the dynamic behavior of the material, with the equilibrium capacity investigated and often only pure component uptakes found. Shen et al.[19] produced breakthrough curves of dilute CO_2 and N_2 streams in helium at low pressure but did not investigate gas mixtures. Casas et al.[20] considered the modeling of the breakthrough curve without investigating the causes for the differences to dynamic response, evaluating the difference in breakthrough times compared to different operating conditions rather than compared to equilibrium data. García et al.[21] studied the separation of $CO_2/H_2/N_2$ mixtures to find the equilibrium adsorption capacity and the breakthrough time of CO_2 uptake compared at different operating conditions, but no equilibrium experiments were performed.

With the majority of investigation into activated carbons for pre-combustion capture focusing on either equilibrium experiments or dynamic experiments, there is limited research comparing these results to dynamic capacities from experimental breakthrough curves. Martin et al.[17] also looked at equilibrium isotherms and dynamic breakthrough experiments but failed to compare the two sets of data. García et al.[18] went on to compare multi-component experimental capacities from breakthrough curves with theoretical capacities predicted from pure component isotherm data. However, the work mainly considered the dual-site Langmuir (DSL) isotherm and did not consider the ideal adsorbed solution theory (IAST).

There is a need for further understanding of high-pressure CO_2 separations with respect to IGCC. The aim of this paper is to report a study of separation of CO_2/N_2 and CO_2/H_2 mixtures at high pressure for the activated carbon beads, comparing the breakthrough capacities to equilibrium results, and to investigate the effect of the CO_2 feed fraction on these results. The novel aspect of this paper is to relate the breakthrough capacity of the materials to the traditional equilibrium adsorption capacity. The IAST has been applied to predict multi-component capacities from pure component isotherm data.

DOI: 10.1021/acs.energyfuels.5b00164
Energy Fuels 2015, 29, 3796−3807

2. EXPERIMENTAL SECTION

2.1. Material Preparation. An unmodified and a modified activated carbon were used in this study. Both materials were prepared by the University of Nottingham, with the preparation techniques of the base activated carbon described by Sun et al.[13] The unmodified activated carbon beads were prepared using a hydrothermal process from phenolic resins. The beads were then activated using mild oxidation at 300 °C for 2 h in air. The modified activated carbons were prepared from the unmodified base by oxidation with nitric acid. The beads were mixed with nitric acid, with a ratio of 10 g of carbon beads to 250 mL of nitric acid, and held at room temperature for 1 h. The oxidized beads were washed and dried before being aminated in a tube furnace under ammonia at 800 °C.

2.2. Surface Area Analysis. Brunauer−Emmett−Teller (BET) analysis was carried out using a Micrometrics ASAP 2420 apparatus to study the textural properties of the activated carbons. Following the method described by Sun et al.,[13] N_2 physisorption was used with nitrogen at −196 °C, following degassing of the sample at 120 °C for 5 h. The results were used to find the surface area, pore volume, and pore diameter for the unmodified and modified activated carbon.

2.3. Adsorption Isotherms. High-pressure isotherms were recorded on both the unmodified and modified activated carbons by the University of Nottingham using the method described by Sun et al.[13] The isotherms were produced by a particulate system high-pressure volumetric analyzer (HPVA-100) using a static volumetric method. The test procedure involved placing approximately 0.5 g of sample into a 2 mL stainless-steel tube. Physisorbed moisture and carbon dioxide were removed by evacuating the system overnight at 120 °C. The sealed sample cell was then transferred to the HPVA, and analysis was performed at a set temperature and pressure up to 40 bar. For the unmodified material, isotherms were found for pure carbon dioxide and pure N_2 streams at 30 and 45 °C. For the modified material, isotherms were recorded for the same gases at 25, 30, 45, and 50 °C.

2.4. Fixed-Bed Experimental Rig. The experimental setup for testing the dynamic response of activated carbon for CO_2/N_2 separations and CO_2/H_2 separations at high pressures is shown in Figure 1. The system was fed by pure CO_2 and either pure N_2 or pure H_2. All of the gases were supplied by BOC Industrial Gases. N_2 gas had a purity of 99.9995% and a bottle pressure of 200 bar; CO_2 had a purity of 99.999% and a bottle pressure of 50 bar; and H_2 used was zero-grade with a purity of 99.995% and a bottle pressure of 200 bar.

The flow of gases was controlled by two Brooks 5850 thermal mass flow controllers. A fixed bed packed with activated carbon was situated inside an oven to control the temperature of the adsorption bed. Temperature programs were used to heat the oven at a set rate, maintain oven temperature, and cool the oven. A Swagelok backpressure regulator was used to control the pressure of the system. The temperatures of the gas up- and downstream of the bed were measured using two K-type thermocouples. A Servomex 5200 multi-purpose portable benchtop gas analyzer, ranging from 0 to 100% CO_2 and an intrinsic error within the system of ±2% of the full-scale range, was used to monitor the concentration of carbon dioxide in the outlet streams. The analyzer was calibrated weekly using pure N_2 for low calibration and a 40% CO_2/N_2 mixture for high calibration as per the recommendations of manufacturer for a maximum reading of 50% CO_2. The same calibration was used replacing N_2 with H_2 for CO_2/H_2 mixtures. The systems in the rig were connected using a $^1/_8$ in. pipe. Two-way valves were used to be able to bypass the bed and the CO_2 analyzer. The temperature and pressure were monitored up- and downstream using temperature probes and pressure transducers.

The bed was made from a stainless-steel pipe, with an internal diameter of 0.025 m, a wall thickness of 0.0015 m, and a length of 0.069 m. The entire bed was filled with the activated carbon adsorbent described in section 2.1, and there was no structure to the packing. The bed density was calculated by dividing weight of the adsorbent added by the volume of the bed. For both the unmodified and modified activated carbon, the same volume of adsorbent was used, and therefore, because of the density differences, the mass of adsorbent in the bed changed.

2.5. Breakthrough Test. Tests were first carried out to determine the response of the pipework without an adsorbent bed fitted, to allow for the dead volume contained in the pipework of the surrounding system in addition to the adsorption bed.

The bed was first fully regenerated to ensure that there was no residual carbon dioxide adsorbed on the active carbon. The system was run under a stream of pure N_2 at 200 N mL min^{-1} for CO_2/N_2 systems at atmospheric pressure. The oven was heated at a rate of 10 °C/min from 25 to 125 °C and then held at 125 °C for 1800 s, before being cooling to 25 °C while maintaining a pure N_2 stream. For CO_2/H_2 systems, pure H_2 was used in place of pure N_2.

The breakthrough experiments were then carried out, where the bed was pressurized under a pure N_2 flow at 200 N mL min^{-1} to 2500 kPa and allowed to equilibrate for 300 s. The flow of N_2 was reduced, and the flow of CO_2 was increased, to give a CO_2 feed fraction of 0.4 while maintaining an overall flow of 200 N mL min^{-1}. The system was allowed to run for 3600 s to ensure that the bed reached full saturation to give the complete breakthrough curve. The bed was then regenerated by switching the feed gas back to a pure N_2 flow of 200 N mL min^{-1}, and the pressure was reduced to atmospheric pressure by opening the backpressure regulator. The bed was held under this pure nitrogen flow for at least 2700 s to ensure all residual CO_2 had been purged from the bed. The breakthrough experiment was repeated 2 more times. Full regeneration by raising the bed temperature as before was not found to be required between each cycle. The experiment was then repeated 3 times for CO_2 mole fractions of 0.1, 0.2, 0.3, and 0.5, including the regeneration step before the first cycle. For CO_2 feed fractions of 0.1 and 0.2, the breakthrough experiment was run for 5400 and 4500 s, respectively. The modified activated carbon was tested for separations of CO_2/N_2 mixtures using the same procedure and repeated for CO_2/H_2 mixtures, where H_2 was used in place of N_2.

3. THEORY

Isotherm equations whose parameters were derived from pure component isotherm data were used to characterize the materials and predict the adsorption capacity for given systems.

3.1. Pure Component Isotherm Equations. Pure component isotherms were obtained in this study by the use of high-pressure volumetric analysis (HPVA) as described in section 2.3. Three pure component isotherm equations were considered here and are shown in Table 1. The Langmuir equation is presented in eq 1; the Langmuir−Freundlich (LF) isotherm is presented in eq 2; and the DSL equation given in eq

Table 1. Pure Component Adsorption Isotherm Equations

Langmuir isotherm	$q_i^* = \frac{q_{s,i} B_i P_i}{(1 + B_i P_i)}$	(1)
LF isotherm	$q_i^* = \frac{q_{s,i} B_i (P_i)^{n_i}}{(1 + B_i (P_i)^{n_i})}$	(2)
DSL isotherm	$q_i^* = \frac{q_{1,s,i} B_{1,i} P_i}{(1 + B_{1,i} P_i)} + \frac{q_{2,s,i} B_{2,i} P_i}{(1 + B_{2,i} P_i)}$	(3)
temperature-independent parameters for LF	$q_{s,i} = k_{1,i}\, e^{k_{2,i}/RT}$	(4)
	$B_i = k_{3,i}\, e^{k_{4,i}/RT}$	(5)
temperature-independent parameters for DSL	$q_{1,s,i} = k_{1,1,i}\, e^{k_{1,2,i}/RT}$	(6)
	$q_{2,s,i} = k_{2,1,i}\, e^{k_{2,2,i}/RT}$	(7)
	$B_{1,i} = k_{1,3,i}\, e^{k_{1,4,i}/RT}$	(8)
	$B_{2,i} = k_{2,3,i}\, e^{k_{2,4,i}/RT}$	(9)

DOI: 10.1021/acs.energyfuels.5b00164
Energy Fuels 2015, 29, 3796−3807

Table 2. Multi-component Adsorption Isotherm Equations

multi-component LF isotherm	$q_i^* = \frac{q_{s,i}B_i(Py_i)^{n_i}}{(1 + \sum_{j=1}^{i} B_j(Py_j)^{n_j})}$	(10)
multi-component DSL isotherm	$q_i^* = \frac{q_{1,s,i}B_{1,i}Py_i}{(1 + \sum_{j=1}^{i} B_{1,j}Py_j)} + \frac{q_{2,s,i}B_{2,i}Py_i}{(1 + \sum_{j=1}^{i} B_{2,j}Py_j)}$	(11)

Table 3. Equations for Applying the IAST to the LF and DSL Equations

IAST base equations	$\frac{\pi_i^0 A}{RT} = \int_0^{p_i^o} \frac{q_i^{\text{pure}}}{p_i} \mathrm{d}p_i$	(12)
	$\frac{1}{q_t} = \sum \frac{x_i}{q_i^{\text{pure}}}$	(13)
	$q_i = x_i q_t$	(14)
IAST−LF equation	$q_{s1} \ln\left(1 + B_1\left(\frac{p_1}{x_1}\right)^{n_1}\right) = q_{s2} \ln\left(1 + B_2\left(\frac{p_2}{1 - x_1}\right)^{n_2}\right)$	(15)
IAST−DSL equation	$q_{1,s1} \ln\left(1 + \frac{B_{1,1}p_1}{x_1}\right) + q_{2,s1} \ln\left(1 + \frac{B_{2,1}p_1}{x_1}\right) = q_{1,s2} \ln\left(1 + \frac{B_{1,2}p_2}{1 - x_1}\right) + q_{2,s2} \ln\left(1 + \frac{B_{2,2}p_2}{1 - x_1}\right)$	(16)

Table 4. BET Surface Measurement Results for the Unmodified and Modified Activated Carbon Material

				wide microporosity[a]		narrow microporosity[b]
	SA_{BET} ($m^2\ g^{-1}$)	V_{total} ($cm^3\ g^{-1}$)	D_{avg} (nm)	SA_{micro} ($m^2\ g^{-1}$)	V_{micro} ($cm^3\ g^{-1}$)	W_0 ($cm^3\ g^{-1}$)
AC	900	0.49	2.19	856	0.36	0.236
MAC	1106	0.49	1.76	1052	0.41	0.237

[a]Calculated by the *t*-plot method. [b]Calculated from CO_2 adsorption at 0 °C by applying the deepest regression (DR) method.

3. The Langmuir and DSL equations are thermodynamically consistent.[22,23] The LF equation does not have the same thermodynamic consistency but has been shown to be applicable to a range of separations. Both the isotherm constant and the saturation capacity were given an Arrhenius temperature dependence for the LF equation, and the DSL equation had temperature-independent parameters found using eqs 4−9.[24] This was performed to allow for application to the breakthrough experiments.

3.2. Multi-component Isotherm Equations. Multi-component equations predicting material capacities for components of gas mixtures requires special isotherm equations because multi-component isotherms are difficult to produce experimentally. Table 2 presents the multi-component isotherm equations studied in this work. Equation 10 is the extended LF equation, and eq 11 is the extended DSL isotherm. Both are based on the original extension of the Langmuir equation, which can be found theoretically.[22] Neither is thermodynamically rigorous because this requires the saturation capacity for all gases to be the same, but this has not previously been applied to the separations studied here. As with the pure component isotherms, the temperature-independent parameters are represented by eqs 4−9. The binary pairs for the DSL isotherm were evaluated on the basis of which configuration gave the greatest adsorption capacity.

3.3. IAST. Instead of using extended pure component equations as detailed in section 3.2, it is possible to apply the IAST, which also uses the pure component data to predict the multi-component capacity.[25] The equations required for calculating the adsorption capacities by the IAST using the LF and DSL isotherms are reported in Table 3. Equation 12 relates the spreading pressure to the equilibrium pressure, which can then be equated for each component. This has been applied to the LF and DSL equations in eqs 15 and 16, respectively. These equations were solved implicitly to find x_i, which was then used in eqs 13 and 14 to give the adsorbent capacity for each component.

4. RESULTS AND DISCUSSION

4.1. Characterization of Adsorbents. BET surface measurements allow for the structural properties of the unmodified and modified activated carbon to be compared. Table 4 shows that the modified material has a significantly greater surface area than the unmodified material as well as a slight increase in the wide microporous volume. Materials with higher surface areas have been shown to have greater adsorption capacities because the physical adsorption that takes place on activated carbon at high pressures is highly dependent upon the surface area.[10,13,26] The total pore volumes for the materials are very similar, and the modified material has a slight reduction in the average pore diameter. The main impact that a reduction in pore size has is an increase in mass-transfer resistance, but only if the pore diffusion is the limiting mass-transfer case.[27]

The densities may be summarized as material density activated carbon (AC), 2040 kg m^{-3}; material density modified activated carbon (MAC), 2069 kg m^{-3}; particle density AC, 500 kg m^{-3}; particle density MAC, 320 kg m^{-3}; bed density AC, 262 kg m^{-3}; and bed density MAC, 191 kg m^{-3}. When packed

DOI: 10.1021/acs.energyfuels.5b00164
Energy Fuels 2015, 29, 3796−3807

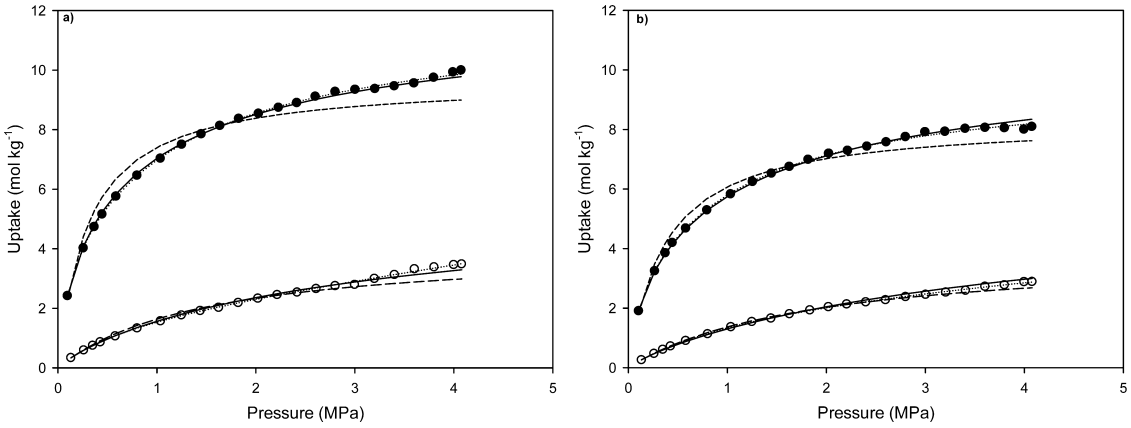

Figure 2. Experimental isotherms for unmodified activated carbon for CO_2 (●) and N_2 (○) at (a) 30 °C and (b) 45 °C and their corresponding isotherm equations: Langmuir (- - -), LF (—), and DSL (···).

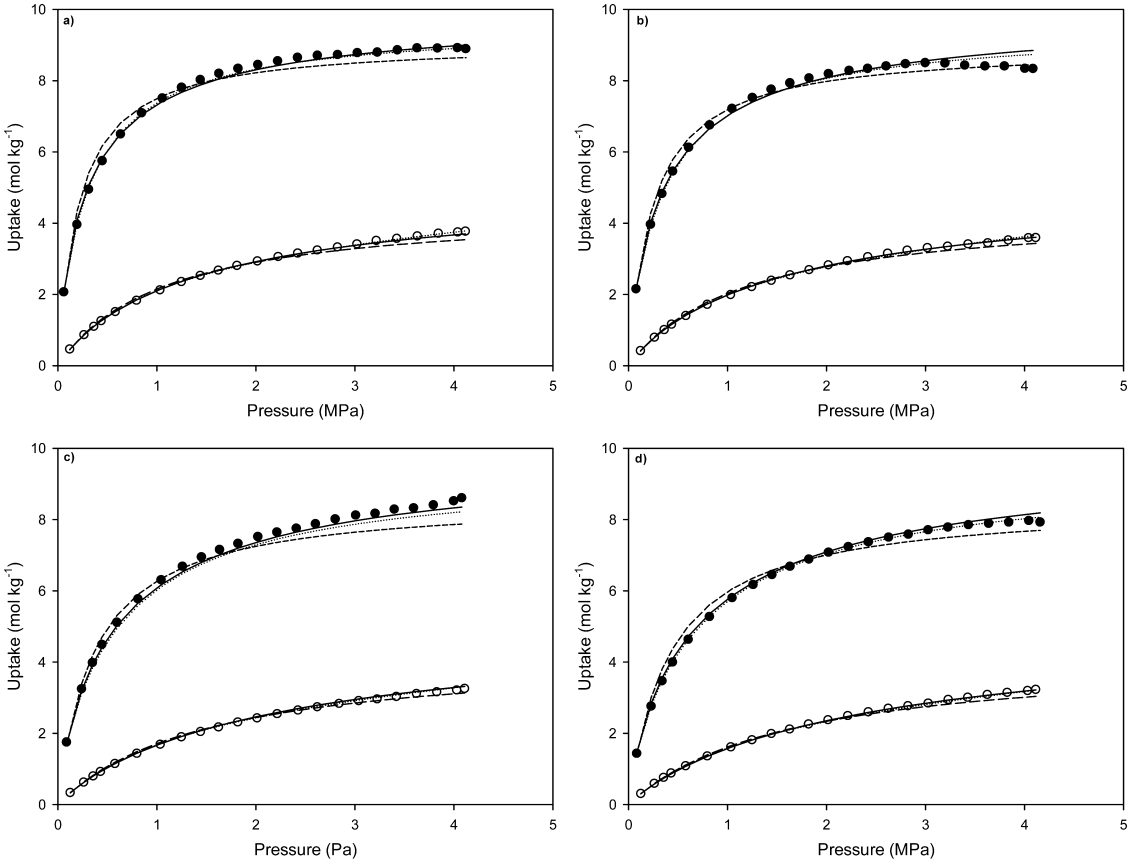

Figure 3. Experimental isotherms for modified activated carbon for CO_2 (●) and N_2 (○) at (a) 25 °C, (b) 30 °C, (c) 45 °C, and (d) 50 °C and their corresponding isotherm equations: Langmuir (- - -), LF (—), and DSL (···).

in the fixed bed, this leads to a bed voidage of AC, 0.48; MAC, 0.4.

4.2. Adsorption Isotherms CO_2/N_2 for Unmodified Activated Carbon. Figure 2 shows the high-pressure isotherm results for N_2 and CO_2 uptakes for the unmodified activated carbon. The isotherm results for the modified activated carbon are shown in Figure 3, where isotherms were measured at four different temperatures. The desorption results are not shown because there is only a small amount of hysteresis, in agreement with Sun et al.[13] For all sets of data, the Langmuir, LF, and DSL isotherms were fitted. From Figures 2 and 3, it is clear that there is little difference between the three equations for the N_2 isotherm. This is because the shape of the isotherm is close to linear, which can be fitted reasonably well with these isotherm equations.[16,18,28] The CO_2 isotherms, on the other hand, are much better fitted by the LF and DSL equations than the Langmuir equation. The Langmuir equation, which literature suggests is suitable at low pressures,[16,18] shows an over-prediction at low pressures and an underprediction at high pressures. The LF equation gives much improved agreement across the whole range of pressures, especially the higher pressures used in pre-combustion capture. Agreement to the LF isotherm is indicative of a heterogeneous activated carbon surface and the high number of interactions with CO_2.[16] The

DOI: 10.1021/acs.energyfuels.5b00164
Energy Fuels 2015, 29, 3796−3807

DSL equation shows much stronger agreement in the high-pressure range than the Langmuir isotherm, indicating that a two-site equation is more suitable than the ideal Langmuir equation. Garcia et al.[18] showed similar agreement between the DSL equation and a CO_2 isotherm on activated carbon, which is again said to give better agreement to the high-pressure region. More complex isotherms, such as the virial isotherm used by Shen et al.,[19] were not used because of the good fit of the LF and DSL isotherms.

The fitted LF parameters and their temperature dependence are shown for the both the unmodified and modified material in Table S1 of the Supporting Information. The temperature dependence of the Langmuir parameter and the saturation capacity can be found fitted to an Arrhenius-type relationship.[15,21,25−27] It was decided to give the saturation capacity a temperature dependence because it gives a better fit across all of the data, with a sum of the squared errors (SSE) of 6.35% for a constant saturation capacity and 1.82% for a temperature dependence for the unmodified material. The parameters for the DSL equation and their temperature dependence are given in Table S2 of the Supporting Information for the unmodified material and Tables S3 and S4 of the Supporting Information for the modified material, again fitted using an Arrhenius-type relationship. Despite the DSL equation itself being thermodynamically rigorous, allowing the saturation capacity to vary with temperature improves the SSE from 3.25 to 1.35% for the unmodified material.

The average values for the CO_2 heat of adsorption were calculated from the Clausius−Clapeyron equation as 24.7 and 26.6 kJ mol^{-1} for the unmodified and modified activated carbons, respectively, and are 14.9 and 15.7 kJ mol^{-1} for N_2, respectively. These are in agreement with literature values for activated carbons, which range from 21 to 30 kJ mol^{-1} for CO_2 and from 10 to 17.5 kJ mol^{-1} for N_2.[16,19,29−35]

4.3. Breakthrough Tests for an Empty Bed. Breakthrough curves were produced for an experimental setup with the fixed bed removed and the surrounding pipes connected directly, to determine the response of the pipework of the system in addition to the bed of the adsorbent itself. The experiment was performed for both CO_2/N_2 mixtures and CO_2/H_2 mixtures to find CO_2 accumulated by the system for both gas mixtures. It was shown that there is a constant increase of 5.1×10^{-6} kmol in the system accumulation for each increase of 0.1 in the feed mole fraction of CO_2 for CO_2/N_2 mixtures and an increase of 4.4×10^{-6} kmol for a feed fraction increase of 0.1 of CO_2 for CO_2/H_2 mixtures. There is also an accumulation for the pipe leading to the mixing junction of 5.6×10^{-6} kmol. The total value for CO_2 captured by the system at each mole fraction is supplied in Table S5 of the Supporting Information and was subtracted from the total capacity found for the fixed-bed adsorption systems to give an accurate amount of CO_2 captured by the fixed bed itself.

4.4. Breakthough Tests for Unmodified Adsorbent with CO_2/N_2. Breakthrough curves for separation of CO_2/N_2 mixtures using unmodified activated carbon were conducted as described in section 2.5. The experimental conditions are given in Table 5. Figure 4 shows the CO_2 breakthrough curves at varying CO_2 feed mole fractions for the unmodified and modified activated carbons. The results are shown at 100 s intervals to distinguish the individual points. The breakthrough time is found by taking the time at which the outlet CO_2 fraction reaches 5% of the inlet CO_2 fraction. As the feed mole fraction increases, a proportional drop in breakthrough time would be expected if the capacity was constant. However, the breakthrough times do not decrease proportionally with the increase in the CO_2 concentration, showing higher adsorption capacities at higher CO_2 feed fractions. This is consistent with the isotherm data, where at higher pressures of CO_2, a larger amount of CO_2 is adsorbed.

Table 5. Experimental Conditions for Separations Using the Unmodified and Modified Activated Carbons

		AC	MAC
bed length	m	0.069	0.065
bed diameter	m	0.025	0.025
pressure	kPa	2500	2500
temperature	K	298	298
feed flow rate	N mL min^{-1}	200	200
adsorbent mass	g	8.88	6.11

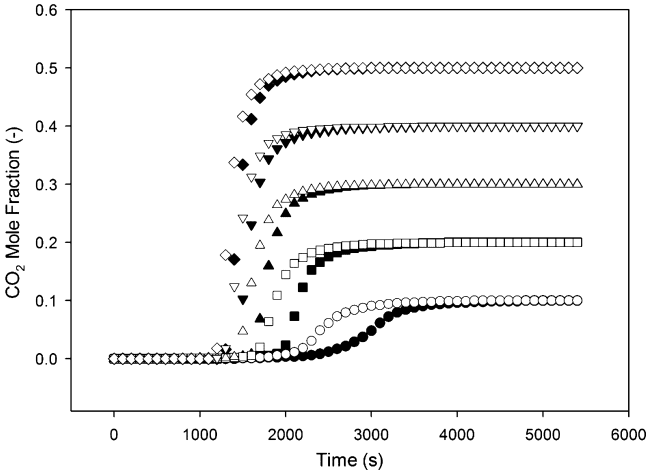

Figure 4. Breakthrough curves for the separation of a CO_2/N_2 mixture using unmodified activated (black) compared to the modified activated carbon material (white).

The shape of the breakthrough curve gives strong indications of the dispersion characteristics and mass-transfer limitations of the system. Systems with large dispersion or mass-transfer resistances have long shallow breakthrough curves.[22] Garg and Ruthven[36] suggest that the shape of the breakthrough curve is affected by both the mass-transfer coefficient and the dispersion coefficient, giving an additive constant to quantify the effect based on both coefficients but without a way to distinguish the contribution of either to it. The steepness of the curves indicates that this effect is relatively small; i.e., neither coefficient is significantly affecting the breakthrough curve. Both the mass-transfer coefficient and the dispersion coefficient are strongly dependent upon gas velocity and particle size.[22] Detailed modeling would be required to differentiate between the two effects. However, the low velocity used in this bed and the relatively small particle size would indicate that both effects should be quite small, as demonstrated by the steepness of the breakthrough curves. The breakthrough for a CO_2 feed fraction of 0.1 sees the greatest amount of spreading. This is to be expected because the residence time is the longest. The error on this reading will also be the highest, and the CO_2 analyzer has an absolute error of ±0.01, leading to a 10% error on the 0.1 run. It is suggested by Garcia et al.[21] that higher pressures lead to greater spreading because of higher degrees of dispersion, but it is not clear if this is attributed to higher absolute pressures or CO_2 partial pressures. This work shows

DOI: 10.1021/acs.energyfuels.5b00164
Energy Fuels 2015, 29, 3796−3807

Table 6. Breakthrough Capacities of CO_2/N_2 Mixtures Separated Using Unmodified Activated Carbon for Each Experimental Run and the Predicted Capacity for Pure Components Based on the LF and DSL Equations

CO_2 feed fraction	breakthrough capacity (mol kg^{-1})	LF equation (mol kg^{-1})	breakthrough capacity as a percentage of LF capacity (%)	DSL equation (mol kg^{-1})	breakthrough capacity as a percentage of DSL capacity (%)
0.1	2.12 ± 0.14	4.38	48.4	4.43	47.9
0.2	4.05 ± 0.15	5.93	68.2	5.94	68.1
0.3	5.01 ± 0.08	6.88	72.8	6.86	73.0
0.4	5.54 ± 0.17	7.55	73.3	7.51	73.7
0.5	6.09 ± 0.06	8.06	75.5	8.02	75.6

Table 7. Predicted Multi-component Adsorption Capacities Based on the Multi-component LF and DSL Equations and the Corresponding IAST Equations for CO_2/N_2 Mixtures Separated Using Unmodified Activated Carbon

		IAST−LF equation (mol kg^{-1})		LF equation (mol kg^{-1})		IAST−DSL equation (mol kg^{-1})		DSL equation (mol kg^{-1})	
CO_2 feed fraction	CO_2 breakthrough capacity (mol kg^{-1})	CO_2	N_2	CO_2	N_2	CO_2	N_2	CO_2	N_2
0.1	2.12 ± 0.14	2.80	0.94	2.88	2.04	2.55	1.11	2.95	1.97
0.2	4.05 ± 0.15	4.49	0.60	4.27	1.66	3.88	0.79	4.75	1.43
0.3	5.01 ± 0.08	5.70	0.40	5.30	1.37	4.82	0.60	5.99	1.06
0.4	5.54 ± 0.17	6.60	0.27	6.12	1.13	5.58	0.46	6.91	0.79
0.5	6.09 ± 0.06	7.30	0.18	6.82	0.91	6.21	0.35	7.62	0.59

that higher partial pressures with a fixed absolute pressure give less mass-transfer and dispersion limitations.

It was observed that there is no significant temperature change at the bed exit, which differs from literature, with Casas et al.[20] seeing increases of up to 40 °C. The breakthrough curve itself suggests that there is an internal temperature change. The steepness of the breakthrough curves and absence of temperature change at the bed exit suggests that any temperature changes are being dissipated very quickly. The distance between the temperature probe and the bed exit would give further chance for the gas to cool.

The breakthrough capacity is found by assuming that all CO_2 input into the system up until the breakthrough time is captured by the system. The system capacities found for the experimental setup without a bed (see Table S5 of the Supporting Information) were subtracted to give the capacity of the bed only. CO_2 that occupies the void space in the bed is also deducted to give the amount of CO_2 that is in the adsorbed phase. The average capacity over 3 cycles is given for each feed fraction in Table 6.

The breakthrough capacity is considered because a PSA system would not be run until complete saturation of the bed, and therefore, a breakthrough capacity is a more realistic prediction of the working capacity of a process unit. The capacity found by the experimental setup will be higher than that of a PSA unit because the bed is fully cleaned between each run. The results show that the increase in breakthrough capacity is larger between lower feed fractions than the highest feed fractions. This is in agreement with the isotherm data, where the feed fractions are proportional to the partial pressure of the gas. By looking at the trend of the isotherm in Figure 2 for the pure component CO_2, an increase in pressure at lower values has a greater increase in capacity than it does at higher pressures. Table 6 also gives the predicted values for the CO_2 capacity for pure component data at the equivalent partial pressure of each component. The isotherm gives a value for equilibrium conditions and also for pure component data, i.e., assuming that N_2 in the mixture does not affect the capacity. The breakthrough capacities approach closer to the equilibrium values as the CO_2 fraction in the feed increases, but even at a CO_2 feed fraction of 0.5, the breakthrough capacity only reaches ∼75% of the pure component capacity. Both of these factors explain the large disparity between the values. The greater difference between the breakthrough capacity and the predicted isotherm value for a feed fraction of 0.1 further emphasizes the larger degree of spreading in the breakthrough curve at the lower feed fractions. The almost constant difference for all other values suggests that the mass-transfer front is well-established for all of those runs.

It is important to find an isotherm equation that can accurately represent the experimental data. The large difference between the isotherm equations and the breakthrough data suggests that the presence of N_2 has a significant impact on the CO_2 capacity, and equations capable of replicating this are required. It is easier to produce pure component isotherm data rather than multi-component data. As discussed in section 3.2, there are several equations that use pure component data to predict multi-component adsorption capacities. Because of the strong agreement for the pure component isotherms shown in section 4.2, the multi-component LF equation and multi-component DSL equation were used to predict the CO_2 capacity. For each of these equations, the IAST was applied to their corresponding pure component results, with the theory behind this discussed in section 3.3. Table 7 compares the predicted capacity for both CO_2 and N_2 by multi-component LF, IAST−LF, multi-component DSL, and IAST−DSL. It can be seen that the various equations differ wildly in their prediction of the CO_2 capacity. IAST−LF predicts a higher capacity for CO_2 than multi-component LF and a lower capacity for N_2. Both equations show considerably higher capacities than the breakthrough capacities. The comparisons in the literature have been to experimental multi-component isotherms, where the IAST equation has been shown to have similar prediction capabilities to multi-component equations.[16,37,38]

The DSL equations show the opposite trend with the IAST−DSL equation predicting lower CO_2 and N_2 capacities than the multi-component DSL equation. The difference may lie in the way that the multi-component system predicts the capacity. Because there are two sites, the way the two component isotherms interact can vary, as explained by Ritter et al.,[39] with the results here given for a positive−positive system. Reversing

DOI: 10.1021/acs.energyfuels.5b00164
Energy Fuels 2015, 29, 3796−3807

Table 8. Predicted Selectivities Based on the Multi-component LF and DSL Equations and the Corresponding IAST Equations for CO_2/N_2 Mixtures Separated Using Unmodified Activated Carbon

CO_2 feed fraction	IAST−LF equation (mol_{CO_2}/mol_{N_2})	LF equation (mol_{CO_2}/mol_{N_2})	IAST−DSL equation (mol_{CO_2}/mol_{N_2})	DSL equation (mol_{CO_2}/mol_{N_2})
0.1	26.8	12.7	20.7	13.5
0.2	29.9	10.3	19.6	13.3
0.3	33.3	9.0	18.7	13.2
0.4	36.7	8.1	18.2	13.1
0.5	40.6	7.5	17.7	12.9

Table 9. Breakthrough Capacities of CO_2/N_2 Mixtures Separated Using Modified Activated Carbon for Each Experimental Run and the Predicted Capacity for Pure Components Based on the LF and DSL Equations

CO_2 feed fraction	breakthrough capacity (mol kg^{-1})	LF (mol kg^{-1})	breakthrough capacity as a percentage of the LF capacity (%)	DSL (mol kg^{-1})	breakthrough capacity as a percentage of the DSL capacity (%)
0.1	2.61 ± 0.13	4.61	56.6	4.53	57.6
0.2	4.67 ± 0.04	6.05	77.2	6.07	76.9
0.3	5.88 ± 0.14	6.83	86.1	6.88	85.5
0.4	6.84 ± 0.16	7.32	93.4	7.39	92.6
0.5	7.48 ± 0.09	7.68	97.4	7.74	96.6

Table 10. Predicted Multi-component Adsorption Capacities Based on the Multi-component LF and DSL Equations and the Corresponding IAST Equations for CO_2/N_2 Mixtures Separated Using Modified Activated Carbon

		IAST−LF equation (mol kg^{-1})		LF equation (mol kg^{-1})		IAST−DSL equation (mol kg^{-1})		DSL equation (mol kg^{-1})	
CO_2 feed fraction	CO_2 breakthrough capacity (mol kg^{-1})	CO_2	N_2	CO_2	N_2	CO_2	N_2	CO_2	N_2
0.1	2.61 ± 0.13	2.74	1.24	2.58	2.27	2.74	1.21	4.48	0.50
0.2	4.67 ± 0.04	4.46	0.77	3.98	1.76	4.38	0.80	6.02	0.27
0.3	5.88 ± 0.14	5.62	0.49	4.98	1.39	5.45	0.57	6.85	0.17
0.4	6.84 ± 0.16	6.43	0.32	5.77	1.09	6.19	0.41	7.37	0.12
0.5	7.48 ± 0.09	7.01	0.21	6.40	0.85	6.73	0.30	7.72	0.08

the interaction of the DSL sites results in a dramatically lower prediction in capacity, and therefore, that equation has been discounted. The IAST equation is underpredicting the breakthrough capacity, with the values for the feed fraction of 0.3 and 0.4 actually being lower than the breakthrough capacity. This may be caused by the IAST equation being unable to take the site interactions into account. The application of the DSL is limited in literature, with the application to the IAST equation even more so. It has previously been applied to activated carbons by Dreisbach et al.;[37] however, a Freundlich-type exponent was included as well. The IAST does not always provide a better fit to multi-component data,[16] and in this case, the data in Table 7 indicate that the IAST equation underpredicts the breakthrough capacity, making the multi-component DSL a better fit.

The selectivity of the material for carbon dioxide can be found using the following equation:[16]

$$S_{CO_2} = \frac{q_{CO_2}/q_{N_2}}{y_{CO_2}/y_{N_2}}$$

Table 8 shows the selectivities for each of the equations. The IAST equations predict a higher selectivity for CO_2, especially at higher CO_2 partial pressures. It is interesting to note that the highest selectivity does not necessarily correspond to the highest predicted carbon dioxide capacity.

For both equations, the solution method that predicts the higher capacity is more likely to be accurate. There is still an appreciable degree of spreading shown in Figure 4, which would suggest that the breakthrough capacity should still be significantly lower than an equilibrium capacity. On this basis, of the equations shown, the IAST−LF and the multi-component DSL equations are the most suitable.

4.5. Modified Activated Carbon Breakthrough Experiments with CO_2/N_2. The experimental setup for the modified material is very similar to the unmodified material and is described in detail in section 2.4. The experimental conditions are given in Table 5. The breakthrough curves for the modified activated carbon are shown in Figure 4 alongside the breakthrough curves for the unmodified material. The shape of the curves shows that there are still very limited mass-transfer and dispersion effects. The breakthrough times are slightly shorter for the modified material. This is mainly due to there being significantly less adsorbent, on a mass basis, in the bed. The difference in density means that the fixed bed for the modified material is almost 50% lighter. The capacity would actually be expected to be considerably less considering the large difference in bed density with only a slight increase in capacity shown by the isotherms. The breakthrough capacity for each run is given in Table 9 as well as a comparison to the pure component capacity, as predicted by the LF and DSL equations. At lower feed fractions, the difference between the breakthrough capacity and the equilibrium capacity is considerable, but this reduces as the CO_2 feed fraction increases. It can be observed that the breakthrough capacity is within 90% of the pure component capacities predicted by the LF and DSL equations for CO_2 feed fractions of 0.4 and 0.5. Because the material has not reached equilibrium at breakthrough, the small differences between the isotherm prediction and the breakthrough capacity can be mainly attributed to this. This suggests that the higher concentration of carbon dioxide and better selectivity mean that the majority

DOI: 10.1021/acs.energyfuels.5b00164
Energy Fuels 2015, 29, 3796−3807

Table 11. Predicted Selectivities Based on the Multi-component LF and DSL Equations and the Corresponding IAST Equations for CO_2/N_2 Mixtures Separated Using Modified Activated Carbon

CO_2 feed fraction	IAST−LF equation (mol_{CO_2}/mol_{N_2})	LF equation (mol_{CO_2}/mol_{N_2})	IAST−DSL equation (mol_{CO_2}/mol_{N_2})	DSL equation (mol_{CO_2}/mol_{N_2})
0.1	19.9	10.2	20.4	80.6
0.2	23.2	9.0	21.9	89.2
0.3	26.8	8.4	22.3	94.0
0.4	30.1	7.9	22.6	92.1
0.5	33.4	7.5	22.4	96.5

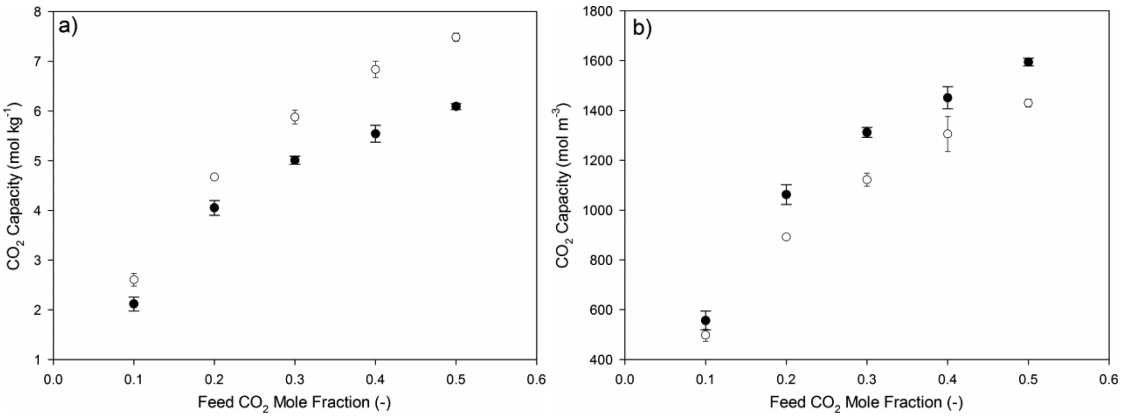

Figure 5. Comparison of unmodified (●) and modified (○) activated carbon breakthrough capacities for the separation of CO_2/N_2 mixtures on (a) mass and (b) volumetric basis.

of the adsorption sites are occupied by carbon dioxide and the interaction by the nitrogen is limited, allowing for the carbon dioxide capacity to approach that of a pure component. Sun et al.[13] discussed the relationship between textural and chemical properties of the materials upon the adsorption capacities. It was shown that adsorption capacities can be largely related to the micropore parameters as opposed to the total pore volume. Micropores contain the majority of sites where CO_2 adsorption occurs, and thus, the CO_2 uptake increases strongly with increasing micropore volume. In terms of surface chemistry, the capacity of the materials could be increased by doping nitrogen into the structure, for example by the addition of melamine, to increase the affinity for CO_2, although such materials are challenging to synthesize as spherical beads.

A similar comparison is made to the multi-component equations for predicting the capacity of the material for each gas and the corresponding selectivity (Tables 10 and 11). The same trend is seen as for the unmodified material, with the multi-component LF and the IAST−DSL predicting lower CO_2 capacities than their counterparts. In this case, the two IAST equations also predict similar CO_2 capacities for all feed fractions. However, the IAST equations and the multi-component LF equation underpredict the breakthrough capacity at higher feed fractions. The multi-component DSL equation is the only equation that predicts a greater equilibrium capacity than the breakthrough capacity for all feed fractions. This is because the predicted N_2 interaction is the least, and therefore, the predicted CO_2 capacities are very similar to the pure component equilibrium prediction. Because the breakthrough capacity results suggest very limited interaction with N_2, this equation most suitably represents the system. This also corresponds to a much higher predicted selectivity for the multi-component DSL equation.

4.6. Comparison of the Capacity of Unmodified and Modified Activated Carbon. A comparison can be made between the breakthrough capacities for each material. In section 4.2, the isotherms show that the unmodified material has slightly greater equilibrium capacities than the modified material. Figure 5a compares the breakthrough capacities of the material on the same mass basis. The modified material outperforms the unmodified activated carbon for all feed fractions, with the greatest difference at higher feed fractions. It is apparent that the selectivity for CO_2 over N_2 is greater for the modified material because the breakthrough capacities are much closer to the pure component equilibrium value. This effect is more apparent at higher CO_2 partial pressures, which might explain the greater difference in breakthrough capacity between the two values at higher feed fractions.

Although the CO_2 capacity on a mass basis is often quoted for materials, it is actually the capacity on a volumetric basis that is more important for a PSA process. However, the unmodified material has a higher bulk density than the modified material, meaning a higher mass of material fits in the same bed volume. The number of moles of CO_2 captured per meter cubed of bed can be found by multiplying the mass capacity by the bulk density of the bed. The results of this are shown in Figure 5b, with the unmodified material greatly outperforming the modified material. This is to be expected because the bulk density is considerably larger for the unmodified material, with only a slight decrease in equilibrium capacity found by the isotherm. This emphasizes the importance of finding the CO_2 capacity on a volumetric basis. Drage et al.[10] indicate this in their evaluation of materials for pre-combustion capture. However, literature values for dynamic capacities are rarely quoted and often on a mass basis for comparison to equilibrium values found from isotherms.[21] The work by Martin et al.[17] briefly comments on this, but the materials being compared show a very limited difference in density and, therefore, in their volumetric capacity. Capacities being quoted on a mass basis instead of a volumetric basis when

DOI: 10.1021/acs.energyfuels.5b00164
Energy Fuels 2015, 29, 3796−3807

found from isotherms also calls into question observations that capacity increases for materials with greater surface area.[10,13] This is true on a mass basis, but often this greater surface area results in a lower density because there needs to be a higher porosity to give the higher surface area. An increase in the surface area is often the focus of modification to activated carbons, which may not have an effect on the volumetric capacity and, therefore, the capacity of a fixed-bed PSA unit.

4.7. CO_2/H_2 Separations over Modified Activated Carbon Beads. For the development of PSA processes for the separation of CO_2 at high pressures, it is important to consider a CO_2/H_2 mixture to ensure that the results of a simulation using CO_2/N_2 would give reasonable indications for applications toward CO_2/H_2 mixtures. Therefore, the fixed-bed experiments were repeated for the modified activated carbon using a CO_2/H_2 gas mixture. The breakthrough curves, given in Figure 6, show that there is a much greater degree of spreading

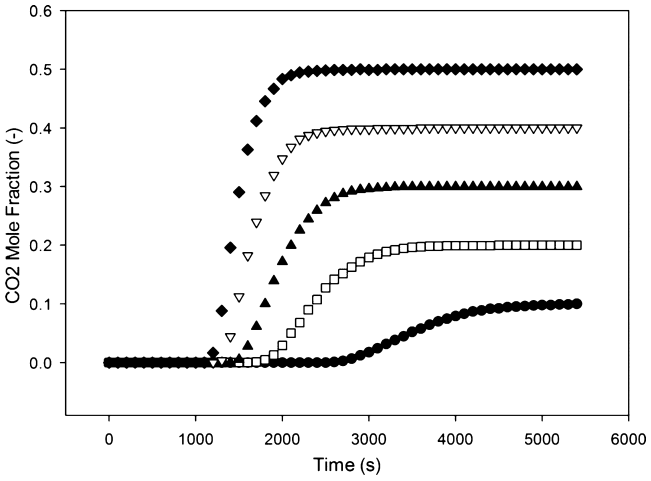

Figure 6. Breakthrough curves for the separation of a CO_2/H_2 mixture using modified activated carbon at CO_2 feed fractions of 0.1 (●), 0.2 (□), 0.3 (▲), 0.4 (▽), and 0.5 (◆).

than for the CO_2/N_2 mixture separations. It is possible to predict the mass-transfer and dispersion coefficients by correlations. The mass-transfer coefficient is based on the three forms of mass transfer taking place, from the bulk to the adsorbent surface, into the macropores, and into the micropores, and each of these is represented by an equation proposed by Farooq and Ruthven.[27] For this system, the rate-limiting step is the mass transfer into the micropores. These are highly system-specific and require complex experiments to find, which were outside the scope of this work. There is no reason for the CO_2 micropore mass-transfer resistance to be affected by the use of H_2 instead of N_2 and, therefore, is likely to be constant for the system. The CO_2 mass-transfer coefficient has a much greater effect on the breakthrough of CO_2 than the H_2 mass-transfer coefficient, and therefore, a change in the H_2 micropore diffusivity is unlikely to noticeably affect the separation. The dispersion coefficient is strongly dependent upon the product of the Reynolds and Schmidt number.[22] The main property that affects this is the diffusivity of the gas mixture. For a CO_2/H_2 mixture, the calculated diffusivity increases,[40] which leads to a decrease in the product of the Reynolds and Schmidt numbers. This typically causes an increase in the dispersion coefficient[22] and explains the greater degree of spreading seen for the breakthrough curves of a CO_2/H_2 mixture than a CO_2/N_2 mixture. A possible limitation of the present work is that pure component HPVA experimental data were only available for CO_2/N_2 mixtures rather than CO_2/H_2 mixtures, and therefore, detailed isotherm parameters could not be derived for CO_2/H_2. A comparison of other studies carried out by Garcia et al.[18] with a similar material AC AP3-60 shows for example that, for a CO_2 mole fraction of 0.3 at 298 K, the fraction of CO_2 captured from a binary CO_2/N_2 mixture divided by the total gas captured is ∼0.818, whereas the fraction of CO_2 captured from a CO/H_2 mixture divided by the total gas captured is ∼0.916, approximately 12% greater than the CO_2/N_2 case. This suggests that the separation of hydrogen can be expected to be higher than the predictions made using nitrogen in the current work. However, real flue gases may contain moisture, which can have an adverse impact upon the separation factors achieved.

5. CONCLUSION

The work presented here gives a complete investigation of two activated carbon materials for the application of high-pressure PSA processes. The isotherms showed that the modified activated carbon had a slightly higher capacity for CO_2 on a mass basis but a lower capacity on a volumetric basis. For both materials, pure component isotherms were fitted and it was found that the LF and DSL equations gave the best fit for CO_2 and N_2. Breakthrough experiments were performed for the separation of CO_2/N_2 mixtures using both materials and for the separation of CO_2/H_2 mixtures using the modified activated carbon. For all breakthrough curves, the mass-transfer and dispersion limitations were found to be minimal, although more significant for the CO_2/H_2 mixtures. In comparison of the capacity of both materials for the separation of CO_2/N_2 mixtures, the modified material was found to have higher CO_2 capacities on a mass basis. However, when these capacities were compared on a volumetric basis, which is more important for PSA applications because it affects the size of the adsorbent bed, the unmodified material had a superior capacity for CO_2. This result shows that the surface area does not have a strong effect on the volumetric capacity, because materials that show higher capacities for CO_2 on a mass basis have sacrificed bulk density to achieve a higher surface area.

Four multi-component isotherm equations were compared to the breakthrough capacities found for the separations of CO_2/N_2 on both materials: multi-component LF, the IAST equation applied to the LF equation, multi-component DSL, and the IAST equation applied to the DSL equation. It was found that the multi-component DSL equation was more suitable because the others underpredicted the CO_2 capacity for the modified material and multi-component LF and IAST−DSL underpredicted the capacity for the unmodified material.

■ ASSOCIATED CONTENT

Supporting Information

LF isotherm values for unmodified and modified activated carbon for N_2 and CO_2 (Table S1), DSL isotherm values for the unmodified activated carbon for N_2 and CO_2 (Table S2), DSL isotherm values for modified activated carbon for N_2 (Table S3), DSL isotherm values for modified activated carbon for CO_2 (Table S4), and response times for the system without a bed at various feed concentrations of CO_2/N_2 given at percentages of the feed concentration (Table S5). The Supporting Information is available free of charge on the

DOI: 10.1021/acs.energyfuels.5b00164
Energy Fuels 2015, 29, 3796−3807

ACS Publications website at DOI: 10.1021/acs.energyfuels.5b00164.

AUTHOR INFORMATION

Corresponding Author

*Telephone: +44-0-121-414-5295. E-mail: j.wood@bham.ac.uk.

Notes

The authors declare no competing financial interest.

ACKNOWLEDGMENTS

The authors are grateful to the Engineering and Physical Sciences Research Council (EPSRC), U.K., for funding under Grant EP/I010955/1.

NOMENCLATURE

A = constant in eq 12 (kg^{-1})
B_i = LF constant component i (Pa^{-n})
$B_{1,i}$ = LF constant component i, dual-site type 1; other equations with two subscripts follow the same convention in eqs 8 and 9 and eqs 15 and 16 (Pa^{-n})
B_j = LF constant component j (Pa^{-n})
D_{avg} = average pore diameter (nm)
P_i = partial pressure of component i
$k_{1,i}$ = constant in temperature dependence equation for $q_{s,i}$ (mol kg^{-1})
$k_{2,i}$ = constant in temperature dependence equation for $q_{s,i}$ (J mol^{-1})
$k_{3,i}$ = constant in temperature dependence equation for B_i (Pa^{-n})
$k_{4,i}$ = constant in temperature dependence equation for B_i (J mol^{-1})
$k_{1,1,i}$ = constant in temperature dependence equation for $q_{1,s,i}$, dual-site type 1; other equations with three subscripts follow the same convention in eqs 6−9 (mol kg^{-1})
n_i = exponent in LF isotherm
p_i = partial pressure of component i (Pa)
P = pressure (Pa)
$q_{1,s,i}$ = component i solid-phase concentration upon dual-site type 1. Other equations with three subscripts follow same convention in eqs 6 and 7 and eqs 15 and 16 (mol kg^{-1})
q_i^* = component solid-phase concentration at equilibrium (mol m^{-3})
q_i^{pure} = component solid-phase concentration of component i with pure i gas phase (mol m^{-3})
q_t = total solid-phase concentration (mol m^{-3})
R = ideal gas constant (J $mol^{-1}K^{-1}$)
S_{CO_2} = selectivity of CO_2 to N_2
SA_{BET} = BET surface area (m^2 g^{-1})
SA_{micro} = surface area contained within micropores (m^2 g^{-1})
T = temperature (K)
V_{micro} = volume contained within micropores (cm^3 g^{-1})
W_0 = narrow microporosity (cm^3 g^{-1})
x_i = mole fraction of component i in the liquid or adsorbed phase
y_i = mole fraction of component i in the gas phase
π_i^0 = spreading pressure of component i under saturation conditions (N m^{-1})

Abbreviations

BET = Brunauer−Emmett−Teller
CCS = carbon capture and storage
DSL = dual-site Langmuir
HPVA = high-pressure volumetric analysis
IAST = ideal adsorbed solution theory
IGCC = integrated gasification combined cycle
PSA = pressure swing adsorption
LF = Langmuir−Freundlich
PSA = Pressure Swing Adsorption
TLC = thin layer chromatography

REFERENCES

(1) European Commission Joint Research Centre (JRC)/Netherlands Environmental Assessment Agency (PBL). *Emission Database for Global Atmospheric Research (EDGAR)*; http://edgar.jrc.ec.europa.eu (accessed July 24, 2013).
(2) Committee on Climate Change. *The Fourth Carbon Budget: Reducing Emissions through the 2020s*; Committee on Climate Change: London, U.K., 2010.
(3) European Commission. *A Roadmap for Moving to a Competitive Low Carbon Economy in 2050*; European Commission: Brussels, Belgium, 2011.
(4) Global CCS Institute. *The Global Status of CCS: 2012*; Global CCS Institute: Canberra, Australia, 2012.
(5) BP. *BP Statistical Review of World Energy 2013*; BP: London, U.K., 2013.
(6) Miller, B. G. *Clean Coal Engineering Technology*; Butterworth-Heinemann: Burlington, MA, 2011.
(7) Figueroa, J.; Fout, T.; Plasynski, S.; McIlvried, H.; Srivastava, R. D. Advances in CO_2 capture technology—The U.S. Department of Energy's Carbon Sequestration Program. *Int. J. Greenhouse Gas Control* **2008**, *2*, 9−20.
(8) Radosz, M.; Hu, X.; Krutkramelis, K.; Shen, Y. Flue-gas carbon capture on carbonaceous sorbents: Toward a low-cost multifunctional carbon filter for "green" energy producers. *Ind. Eng. Chem. Res.* **2008**, *47* (10), 3783−3794.
(9) Cormos, C.-C. Evaluation of energy integration aspects for IGCC-based hydrogen and electricity co-production with carbon capture and storage. *Int. J. Hydrogen Energy* **2010**, *35* (14), 7485−7497.
(10) Drage, T. C.; Blackman, J. M.; Pevida, C.; Snape, C. E. Evaluation of activated carbon adsorbents for CO_2 capture in gasification. *Energy Fuels* **2009**, *23* (5), 2790−2796.
(11) Chen, Z.; Deng, S.; Wei, H.; Wang, B.; Huang, J.; Yu, G. Activated carbons and amine-modified materials for carbon dioxide capture—A review. *Front. Environ. Sci. Eng.* **2013**, *7* (3), 326−340.
(12) Sircar, S.; Golden, T. C.; Rao, M. B. Activated carbon for gas separation and storage. *Carbon* **1996**, *34* (1), 1−12.
(13) Sun, N.; Sun, C.; Liu, H.; Liu, J.; Stevens, L.; Drage, T.; Snape, C. E.; Li, K.; Wei, W.; Sun, Y. Synthesis, characterization and evaluation of activated spherical carbon materials for CO_2 capture. *Fuel* **2013**, *113*, 854−862.
(14) Casero, P.; Pena, F. G.; Coca, P.; Trujillo, J. ELCOGAS 14 MW_{th} pre-combustion carbon dioxide capture pilot. Technical & economical achievements. *Fuel* **2014**, *116*, 804−811.
(15) Drage, T. C.; Kozynchenko, O.; Pevida, C.; Plaza, M. G.; Rubiera, F.; Pis, J. J.; Snape, C. E.; Tennison, S. Developing activated carbon adsorbents for pre-combustion CO_2 capture. *Energy Procedia* **2009**, *1*, 599−605.
(16) Schell, J.; Casas, N.; Pini, R.; Mazzotti, M. Pure and binary adsorption of CO, H_2, and N_2 on activated carbon. *Adsorption* **2012**, *18* (1), 49−65.
(17) Martín, C. F.; García, S.; Beneroso, D.; Pis, J. J.; Rubiera, F.; Pevida, C. Precombustion CO_2 capture by means of phenol−formaldehyde resin-derived carbons: From equilibrium to dynamic conditions. *Sep. Purif. Technol.* **2012**, *98*, 531−538.
(18) Garcia, S.; Pis, J. J.; Rubiera, F.; Pevida, C. Predicting mixed-gas adsorption equilibria on activated carbon for precombustion CO_2 capture. *Langmuir* **2013**, *29* (20), 6042−6052.
(19) Shen, C.; Grande, C. A.; Li, P.; Yu, J.; Rodrigues, A. E. Adsorption equilibria and kinetics of CO2 and N2 on activated carbon beads. *Chemical Engineering Journal* **2010**, *160* (2), 398−407.

DOI: 10.1021/acs.energyfuels.5b00164
Energy Fuels 2015, 29, 3796−3807

(20) Casas, N.; Schell, J.; Pini, R.; Mazzotti, M. Fixed bed adsorption of CO_2/H_2 mixtures on activated carbon: Experiments and modeling. *Adsorption* **2012**, *18* (2), 143−161.
(21) García, S.; Gil, M. V.; Martín, C. F.; Pis, J. J.; Rubiera, F.; Pevida, C. Breakthrough adsorption study of a commercial activated carbon for pre-combustion CO_2 capture. *Chem. Eng. J.* **2011**, *171* (2), 549−556.
(22) Ruthven, D. M. *Principles of Adsorption and Adsorption Processes*; John Wiley & Sons, Inc.: New York, 1984.
(23) Myers, A. L.; Prausnitz, J. M. Thermodynamics of mixed-gas adsorption. *AIChE J.* **1965**, *11* (1), 121−127.
(24) Do, D. D. *Adsorption Analysis: Equilibria and Kinetics*; Imperial College Press: London, U.K., 1998.
(25) Rouquerol, F.; Roquerol, J.; King, K. S. W. *Adsorption by Powders and Porous Solids: Principles, Methodology, and Applications*; Academic Press: San Diego, CA, 1999.
(26) Siriwardane, R. V.; Shen, M.-S.; Fisher, E. P.; Poston, J. A. Adsorption of CO_2 on molecular sieves and activated carbon. *Energy Fuels* **2001**, *15*, 279−284.
(27) Farooq, S.; Ruthven, D. M. Heat effects in adsorption column dynamics. 2. Experimental validation of the one-dimensional model. *Ind. Eng. Chem. Res.* **1990**, *29* (6), 1084−1090.
(28) Park, J.-H.; Kim, J.-N.; Cho, S.-H.; Kim, J.-D.; Yang, R. T. Adsorber dynamics and optimal design of layered beds for multicomponent gas adsorption. *Chem. Eng. Sci.* **1998**, *53* (23), 3951−3963.
(29) Agarwal, A.; Biegler, L. T.; Zitney, S. E. Superstructure-based optimal synthesis of pressure swing adsorption cycles for precombustion CO_2 capture. *Ind. Eng. Chem. Res.* **2009**, *49* (11), 5066−5079.
(30) Chue, K. T.; Kim, J. N.; Yoo, Y. J.; Cho, S. H.; Yang, R. T. Comparison of activated carbon and zeolite 13X for CO_2 recovery from flue gas by pressure swing adsorption. *Ind. Eng. Chem. Res.* **1995**, *34* (2), 591−598.
(31) Dantas, T. L. P.; Luna, F. M. T.; Silva, I. J., Jr.; de Azevedo, D. C. S.; Grande, C. A.; Rodrigues, A. E.; Moreira, R. F. P. M. Carbon dioxide−nitrogen separation through adsorption on activated carbon in a fixed bed. *Chem. Eng. J.* **2011**, *169* (1−3), 11−19.
(32) Salem, M. M. K.; Braeuer, P.; Szombathely, M. v.; Heuchel, M.; Harting, P.; Quitzsch, K.; Jaroniec, M. Thermodynamics of high-pressure adsorption of argon, nitrogen, and methane on microporous adsorbents. *Langmuir* **1998**, *14* (12), 3376−3389.
(33) Grande, C. A.; Blom, R.; Möller, A.; Möllmer, J. High-pressure separation of CH_4/CO_2 using activated carbon. *Chem. Eng. Sci.* **2013**, *89*, 10−20.
(34) Himeno, S.; Komatsu, T.; Fujita, S. High-pressure adsorption eqeuilbria of methane and carbon dioxide on several activated carbons. *J. Chem. Eng. Data* **2005**, *50*, 369−376.
(35) Lopes, F. V. S.; Grande, C. A.; Rodrigues, A. E. Activated carbon for hydrogen purification by pressure swing adsorption: Multicomponent breakthrough curves and PSA performance. *Chem. Eng. Sci.* **2011**, *66*, 303−317.
(36) Garg, D. R.; Ruthven, D. M. Performance of molecular sieve adsorption columns: Combined effects of mass transfer and longitudinal diffusion. *Chem. Eng. Sci.* **1975**, *30* (9), 1192−1194.
(37) Dreisbach, F.; Staudt, R.; Keller, J. U. High pressure adsorption data of methane, nitrogen, carbon dioxide and their binary and ternary mixtures on activated carbon. *Adsorption* **1999**, *5* (3), 215−227.
(38) Rother, J.; Fieback, T. Multicomponent adsorption measurements on activated carbon, zeolite molecular sieve and metal−organic framework. *Adsorption* **2013**, *19* (5), 1065−1074.
(39) Ritter, J. A.; Bhadra, S. J.; Ebner, A. D. On the use of the dual-process Langmuir model for correlating unary equilibria and predicting mixed-gas adsorption equilibria. *Langmuir* **2011**, *27* (8), 4700−4712.
(40) Bird, R. B.; Stewart, W. E.; Lightfoot, E. N. *Transport Phenomena*, 2nd ed.; John Wiley & Sons, Inc.: Chichester, U.K., 2001.

DOI: 10.1021/acs.energyfuels.5b00164
Energy Fuels 2015, 29, 3796−3807